Electron-Nuclear Entanglement in the Time-Dependent Molecular Wavefunction

Federica Agostini[a], E. K. U. Gross[b,c], Basile F. E. Curchod[d]

[a]*Laboratoire de Chimie Physique, UMR 8000 CNRS/University Paris-Sud, 91405 Orsay, France*
[b]*Max-Planck-Institut für Mikrostrukturphysik, Weinberg 2, D-06120 Halle, Germany*
[c]*Fritz Haber Center for Molecular Dynamics, Institute of Chemistry, The Hebrew University of Jerusalem, Jerusalem 91904, Israel*
[d]*Department of Chemistry, Durham University, South Road, Durham DH1 3LE, United Kingdom*

Abstract

We address the problem of electron-nuclear entanglement in time-dependent molecular wavefunctions, key quantities of quantum nonadiabatic molecular dynamics. The most natural way of tackling this question consists in comparing the nonadiabatic dynamics obtained from time-dependent self-consistent field and the exact factorization of the time-dependent electron-nuclear wavefunction. Both approaches are based on a single-product Ansatz for the molecular wavefunction, with both a time-dependent electronic and nuclear wavefunction. In the former, however, electron-nuclear coupling is treated within the mean-field approximation, whereas in the latter the entanglement is completely accounted for. Based on a numerical model study, we analyze the nature of the electron-nuclear entanglement in the exact factorization.

Keywords: Electron-nuclear entanglement, Nonadiabatic dynamics, Excited-state dynamics, Ehrenfest dynamics, Exact factorization

1. Introduction

The mean-field approach is widely used in the fields of theoretical chemistry and chemical physics for electronic structure [1, 2] and nuclear

Email addresses: federica.agostini@u-psud.fr (Federica Agostini), basile.f.curchod@durham.ac.uk (Basile F. E. Curchod)

dynamics calculations [2, 3, 4, 5]. The major drawback of this strategy resides in its lack of correlation, or entanglement, among the degrees of freedom treated within the mean-field approximation. The purpose of this work is to propose a different perspective on this concept, the electron-nuclear entanglement, in the context of the time-dependent molecular wave-function, thus employing the time-dependent self-consistent field (TDSCF) scheme [6, 7, 8, 9]. Specifically, here we refer to TDSCF as the approximation used to describe the electron-nuclear coupling in the molecular wavefunction, rather than as a particular numerical procedure.

TDSCF allows to perform calculations on large molecular systems, effectively reducing the "exponential complexity" of the exact quantum-mechanical problem. For an increasing number of degrees of freedom, it might be expected that the mean-field approximation becomes more and more accurate. In addition, the choice of coordinates used to describe the problem plays an important role [10, 11, 12], even though the difficulty lies on the definition of a systematic way to select the appropriate set of variables for which the mean-field description is adequate. TDSCF, especially in its quantum-classical version [13, 14, 15, 16], *i.e.*, the Ehrenfest approach, is often employed for excited-state molecular dynamics, in particular for the early dynamics following photoionization (see for example Ref. [17]). However, the underlying treatment of quantum decoherence [18, 19, 20, 21, 22] and energy exchange mechanisms [23, 24, 25, 26, 27] is sometimes a source of debate. Ehrenfest dynamics is also sometimes used in combination with more advanced strategies for nonadiabatic dynamics [28], for example as a mean to propagate a time-dependent basis for the nuclear wavefunction [29, 30].

Rather than analyzing the quality of the mean-field approximation, which clearly depends on the problem at hand and as such cannot be generally assessed, our purpose here is to investigate the *nature* of the missing entanglement between electronic and nuclear degrees of freedom. To this end, we compare TDSCF with the time-dependent version of the exact factorization of the electron-nuclear wavefunction [31, 32]. The focus will be put on the Ansatz for the molecular wavefunction, and on the corresponding equations of motion derived for the two components of the total wavefunction. In previous work, the exact factorization has been compared to the Born-Oppenheimer approximation [33, 34, 35] and to the Born-Huang expansion [36, 37, 38, 39], but the relation between TDSCF and exact factorization is still lacking. It seems natural, however, to investigate their

connection, since the formal structure of the molecular wavefunction, represented as a single product of an electronic and a nuclear wavefunction, lends itself for a direct comparison.

We start our analysis by addressing the concept of electron-nuclear entanglement from a quantum-mechanical perspective, in Section 2, and then by discussing the effect of the quantum-classical approximation, in Section 3. Our observations are supported by calculations performed on a model test system representing a nonadiabatic proton-coupled electron transfer. Conclusions are summarized in Section 4.

2. Definition of electron-nuclear entanglement

Electron-nuclear entanglement can be defined as everything that cannot be described by the TDSCF approximation [6, 7, 13, 5] of the molecular wavefunction:

$$\Psi_{\mathrm{TDSCF}}(\mathbf{r},\mathbf{R},t) = \chi(\mathbf{R},t)\Phi(\mathbf{r},t). \tag{1}$$

Here, $\chi(\mathbf{R},t)$ is the nuclear wavefunction, depending on the nuclear coordinates $\mathbf{R}$, whereas $\Phi(\mathbf{r},t)$ is the electronic wavefunction with $\mathbf{r}$ describing the electronic coordinates. Both components of the full wavefunction depend on time, making this Ansatz suited to describe electronic excited-state dynamics. However, the coupling between electronic and nuclear motion can be treated only approximately, in a mean-field fashion, as intensively discussed in the literature (see Ref. [13] for example). In its exact form, the electron-nuclei coupling should, in principle, account for the effects on the nuclear evolution resulting from changes in electronic-state occupations (and coherences), and for the role of nuclear dynamics in inducing those changes. The TDSCF approximation is likely to miss some of these critical effects. Therefore, *how can the electron-nuclear entanglement in the product form of the full wavefunction be restored?* Comparing Eq. (1) with the exact form of the electron-nuclear wavefunction [31, 32, 40],

$$\Psi(\mathbf{r},\mathbf{R},t) = \chi(\mathbf{R},t)\Phi_{\mathbf{R}}(\mathbf{r},t), \tag{2}$$

suggests that the parametric dependence of the electronic wavefunction $\Phi_{\mathbf{R}}(\mathbf{r},t)$ on nuclear positions is everything that is needed to fully account for electron-nuclear entanglement. In fact, this "correlated-product" form has been shown to yield exactly the full wavefunction at all times, provided that $\Phi_{\mathbf{R}}(\mathbf{r},t)$ is normalized to one $\forall\,\mathbf{R},t$ (partial normalization condition, PNC), and that the evolution equations for $\Phi_{\mathbf{R}}(\mathbf{r},t)$ and $\chi(\mathbf{R},t)$

are determined from the full time-dependent Schrödinger equation (for $\Psi(\mathbf{r}, \mathbf{R}, t)$). The symbol used in Eq. (2) for the nuclear wavefunction is the same as in Eq. (1), even though the two functions can be very different from one another, as shown below. In both cases, the nuclear density $|\chi|^2$ can be determined by integrating $|\Psi|^2$ (or $|\Psi_{\mathrm{TDSCF}}|^2$) over electronic variables.

We will analyze the two forms of the time-dependent molecular wavefunction based on a model for nonadiabatic proton-coupled electron transfer [41]. The details of the system Hamiltonian and the simulations are given in Appendix A. The model is one-dimensional; thus, we will drop the bold symbols henceforth for $\mathbf{r}$ and $\mathbf{R}$.

The exact wavefunction $\Psi(r, R, t)$ is obtained by solving the full time-dependent Schrödinger equation,

$$i\hbar\partial_t \Psi(r, R, t) = \hat{H}\Psi(r, R, t). \tag{3}$$

Here, $\hat{H}(r, R) = \hat{T}_n(R) + \hat{T}_e(r) + \hat{V}(r, R)$, where $\hat{T}_n$ is the nuclear kinetic energy, $\hat{T}_e$ is the electronic kinetic energy, and $\hat{V}$ the interaction potential. In the following, we will also use the symbol $\hat{H}_{BO} = \hat{T}_e + \hat{V}$ to indicate the electronic Born-Oppenheimer (BO) Hamiltonian. $\Psi_{\mathrm{TDSCF}}(r, R, t)$ is constructed by solving the coupled equations

$$i\hbar\partial_t \tilde{\Phi}(r, t) = \left[\hat{T}_e + \langle \hat{V} \rangle_\chi\right] \tilde{\Phi}(r, t) \tag{4}$$

$$i\hbar\partial_t \chi(R, t) = \left[\hat{T}_n + \langle \hat{V} \rangle_{\tilde{\Phi}}\right] \chi(R, t). \tag{5}$$

The symbols $\langle \cdot \rangle_\chi$ and $\langle \cdot \rangle_{\tilde{\Phi}}$ stand for an average operation over the instantaneous nuclear or electronic wavefunction, respectively. Therefore, Eq. (4) describes the evolution of the electronic wavefunction in the mean field created by the nuclei, whereas the nuclei move according to Eq. (5) in the mean field of the electrons. In addition, note that, in order to obtain this form of the TDSCF equations (the procedure is described in Appendix B), we have multiplied $\Phi(r, t)$ by a purely time-dependent phase, namely

$$\tilde{\Phi}(r, t) = e^{\frac{i}{\hbar}\int_0^t dt' E_{BO}(t')} \Phi(r, t), \tag{6}$$

with $E_{BO}(t) = \langle \Phi(t) | i\hbar\partial_t | \Phi(t) \rangle_r$ [13, 21]. The symbol $\langle \cdot \rangle_r$ is used to indicate an integration over the electronic variable.

Comparing the dynamics resulting from the TDSCF to the exact-propagation one will allow us to point out the qualitative features that are missing as a consequence of the mean-field character of the electron-nuclear coupling. To identify the source of the qualitative disagreement, we will focus on the equations that generate the time evolution in the approximate, TDSCF case, and in the exact, factored form.

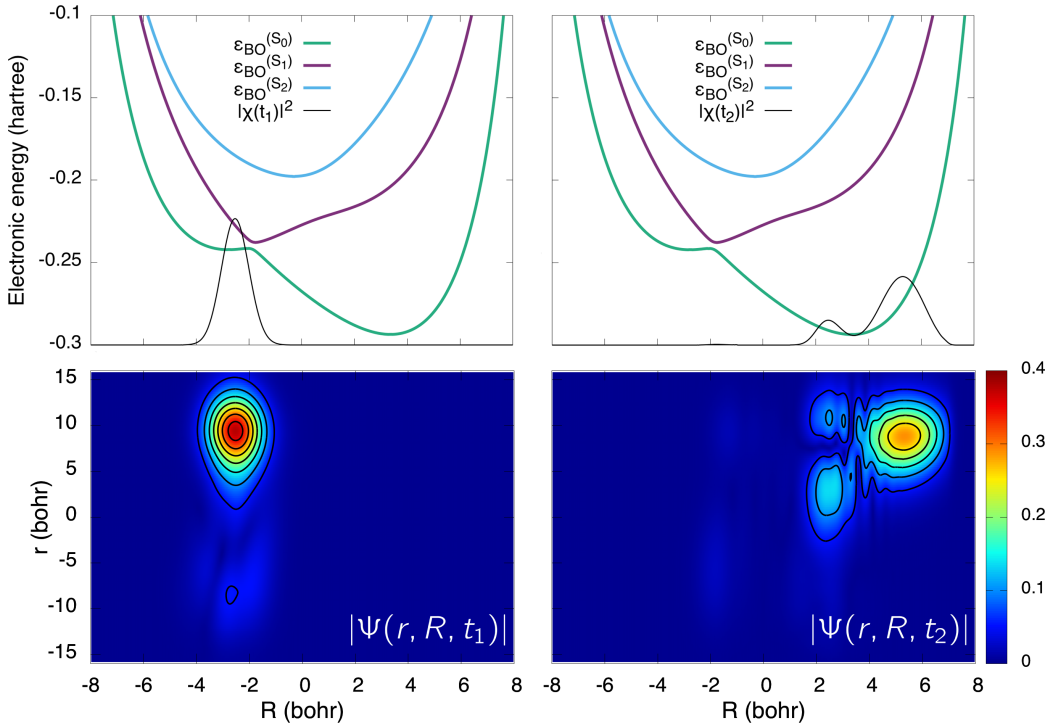

Figure 1: Results of the propagation using the exact time-dependent Schrödinger equation. Upper panels: the three lowest adiabatic PESs for a proton-coupled electron transfer model (ground state S_0, green curve, first excited state S_1, palatinate curve, second excited state S_2, cyan curve). The nuclear density is shown as a black line at times $t_1 = 10.8$ fs (left) and $t_2 = 31.2$ fs (right). Lower panels: modulus of the molecular wavefunction, $|\Psi(r, R, t)|$, at times $t_1 = 10.8$ fs (left) and $t_2 = 31.2$ fs (right).

Fig. 1 (upper panels) shows three adiabatic potential energy surfaces (PESs), *i.e.*, the eigenvalues of $\hat{H}_{BO}$ as functions of R. The two lowest surfaces, $\epsilon_{BO}^{(S_0)}(R)$ and $\epsilon_{BO}^{(S_1)}(R)$, present an avoided crossing at about $R_{ac} = -2.0$ bohr. Therefore, when the nuclear wavepacket, prepared at the initial time on $\epsilon_{BO}^{(S_1)}$ centered at $R_0 = -4$ bohr, passes through the avoided cross-

ing, population transfer from S_1 to S_0 is observed. The resulting nuclear dynamics is shown at times $t_1 = 10.8$ fs (upper left panel of Fig. 1) and $t_2 = 31.2$ fs (upper right panel of Fig. 1), when the nuclear density is close to the avoided crossing and after the transfer is completed, respectively. For the very same times, Fig. 1 (lower panels) shows the modulus of the full molecular wavefunction, $|\Psi(r, R, t)|$. Notice how the two-dimensional distribution of $\Psi(r, R, t)$ mirrors the different structures of the nuclear density. At time t_1, the nuclear probability density is unimodal, approximately localized between $R = -1$ bohr and $R = -4$ bohr, while $|\Psi(r, R, t)|$ is mainly peaked between 0 and $r = 15$ bohr, along the electronic coordinate. At later times, t_2 in Fig. 1, population has transferred from S_1 to S_0, the nuclear density is now bimodal, and a more complex structure of $|\Psi(r, R, t)|$ emerges along the electronic component: for R between 4 and 8 bohr, the probability distribution along the electronic coordinate has a single-peak shape, while for R between 1 and 4 bohr, two main peaks can be observed. Such (abrupt) change of character for $|\Psi(r, R, t)|$ suggests that the two portions of the nuclear density, and thus of the nuclear wavepacket, are associated to different electronic characters. We will now show that this feature cannot be captured by the TDSCF form of the full wavefunction.

Within the TDSCF approximation, the molecular wavefunction is constructed as the product of an electronic and a nuclear wavefunction, respectively evolved according to Eqs. (4) and (5). For the same times presented in Fig. 1, t_1 and t_2, we report in Fig. 2 the results of the TDSCF propagation. At time t_1 (left panels of Fig. 2), only the distribution $|\Psi_{\mathrm{TDSCF}}(r, R, t)|$ along the electronic coordinate shows a small difference in the negative r-region when compared to the exact result of Fig. 1. However, at a later time t_2, a qualitative difference with the exact result is observed in the nuclear density (upper panel), which translates in a very different shape of $|\Psi_{\mathrm{TDSCF}}(r, R, t)|$ as compared to $|\Psi(r, R, t)|$. The TDSCF nuclear density, despite being well localized in the positive R-region between 2 and 8 bohr, has an unimodal distribution. Therefore, the abrupt change of character along the r-direction, previously observed in $|\Psi(r, R, t)|$, is suppressed within the mean-field approximation. At this stage, a question naturally arises: *How can the source of this disagreement be identified?* As the lack of the appearance of a bimodal nuclear distribution can only be rooted in the difference between $|\Psi_{\mathrm{TDSCF}}(r, R, t)|$ and $|\Psi(r, R, t)|$, we shall look in detail at the equations of motion for the nuclear wavefunctions in the TDSCF

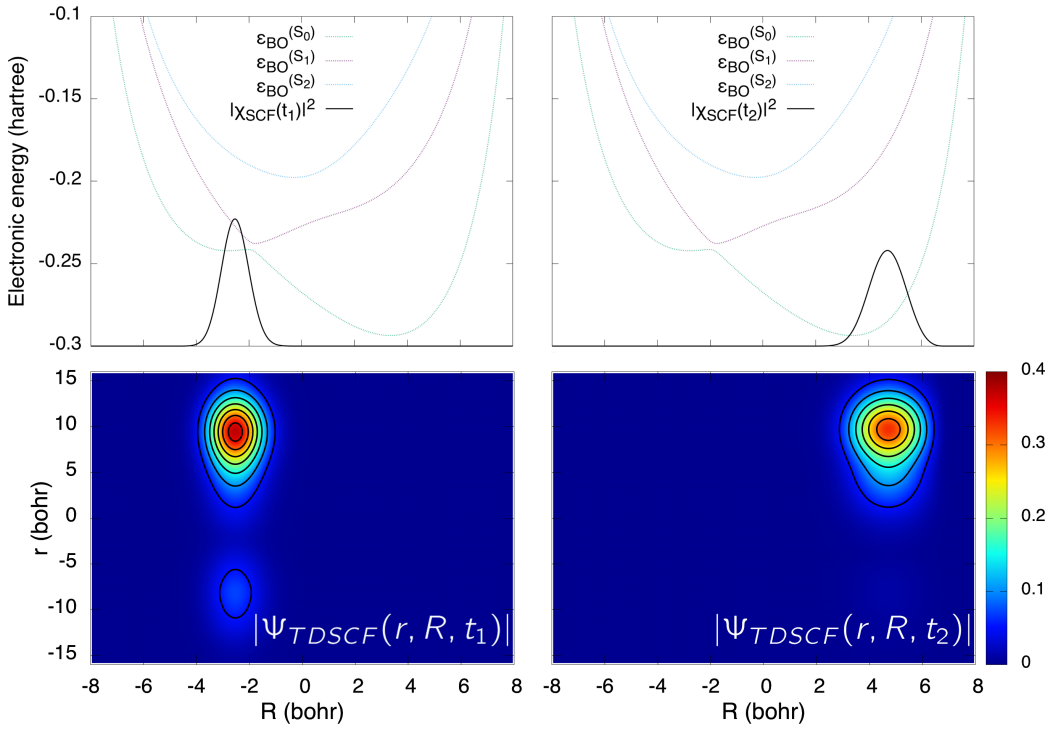

Figure 2: Results of the propagation using the TDSCF approximation. The panels show similar quantities as in Fig. 1.

approximation and in the exact factored form of the full wavefunction.

When the exact product form of the molecular wavefunction in Eq. (2) is inserted into the time-dependent Schrödinger equation (3), the evolution equations

$$i\hbar\partial_t \Phi_R(r,t) = \left[\hat{T}_e + \hat{V} + \hat{U}_{en}[\chi] - \epsilon(R,t)\right] \Phi_R(r,t) \quad (7)$$

$$i\hbar\partial_t \chi(R,t) = \left[\hat{T}_n + \epsilon(R,t)\right] \chi(R,t) \quad (8)$$

are derived by imposing the PNC. The electron-nuclear coupling operator is $\hat{U}_{en}[\chi] = (-i\hbar\partial_R)^2/(2M) - i\hbar\partial_R\chi/(M\chi)(-i\hbar\partial_R)$.

These equations have been reported here in a particular gauge. The product form of the full wavefunction in Eq. (2) is invariant under a (R,t)-dependent phase transformation, which represents the only freedom in determining the electronic and nuclear wavefunctions. If a condition is given to fix this gauge freedom, the solutions of Eqs. (7) and (8) are unique.

Here, the choice of gauge (as detailed in Appendix A) is made to ensure that the nuclear Hamiltonian of Eq. (8) only contains a time-dependent scalar potential, or time-dependent potential energy surface (TDPES), as a generator of the nuclear dynamics.[1]

The TDPES in Eq. (8) has an expression strikingly similar to the potential energy term $\langle \hat{V} \rangle_{\tilde{\Phi}}$ in Eq. (5). The expression of the TDPES is obtained by multiplying Eq. (7) by $\Phi_R^*(r,t)$ and integrating over the electronic variable, that is

$$\begin{aligned} \epsilon(R,t) &= \langle \Phi_R(t)| \, \hat{T}_e + \hat{V} \, |\Phi_R(t)\rangle_r + \frac{\hbar^2}{2M} \langle \partial_R \Phi_R(t)| \, \partial_R \Phi_R(t)\rangle_r \\ &\quad - \langle \Phi_R(t)| \, i\hbar\partial_t \, |\Phi_R(t)\rangle_r \, , \end{aligned} \tag{9}$$

while in Eq. (5) the corresponding potential is

$$\langle \hat{V} \rangle_{\tilde{\Phi}} = \langle \hat{V} \rangle_{\Phi} = \langle \Phi(t)| \, \hat{T}_e + \hat{V} \, |\Phi(t)\rangle_r \, . \tag{10}$$

Note that in Eq. (10) the average of $\hat{T}_e$ on $\Phi(r,t)$ yields a constant function of R, thus it does not have any effect on the dynamics.

We will now compare the first term on the right-hand side of Eq. (9) to the formally identical term in Eq. (10). It is worth recalling [33] here that the second term on the right-hand side of Eq. (9) is negligible if compared to the other two, as it is $\mathcal{O}(M^{-1})$, and will not alter in any way the analysis we will report shortly. The last term in Eq. (9), on the other hand, can have a strong R-dependence and, thus, can have an important effect on the dynamics. This point has been already extensively discussed in previous work [37, 36, 38]. Hence, comparing side by side $\langle \Phi(t)| \, \hat{T}_e + \hat{V} \, |\Phi(t)\rangle_r$ to $\langle \Phi_R(t)| \, \hat{T}_e + \hat{V} \, |\Phi_R(t)\rangle_r$ will allow us to investigate the influence of the R-dependence encoded in the exact electronic wavefunction.

Fig. 3 shows the (first two terms of the) exact TDPES and the TDSCF potential, i.e., $\langle \hat{V} \rangle_{\Phi}$, at times t_1 (left panel) and t_2 (right panel) and clearly shows the crucial importance of the parametric R dependence in the electronic wavefunction. Formally, the two mathematical expressions are the

[1] In general, a time-dependent vector potential also appears in Eq. (8), but the choice of gauge introduced here guarantees that the vector potential is identically zero. This choice can always be made in one-dimensional situations, but cannot be generalized in higher dimensions [42, 43].

same: the average of the electronic BO Hamiltonian $\hat{H}_{BO} = \hat{T}_e + \hat{V}$ over the time-dependent electronic wavefunction. However, the two curves largely differ from each other. At time t_1, the TDPES and $\langle \hat{V} \rangle_\Phi$ are very similar in

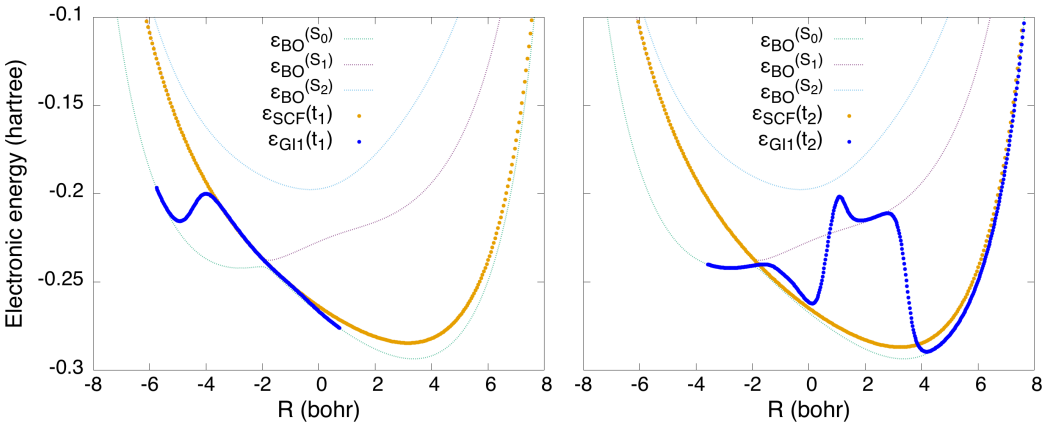

Figure 3: Comparison between $\epsilon_{\rm SCF}(R,t) = \langle \hat{V} \rangle_\Phi(R,t)$ of Eq. (10) (orange dots) and the first two terms, named $\epsilon_{GI}(R,t)$, on the right-hand side of Eq. (9) (blue dots), at times $t_1 = 10.8$ fs (left panel) and $t_2 = 31.2$ fs (right panel). $\epsilon_{GI}(R,t)$ is the gauge-invariant part of the TDPES as it is not affected by the change of gauge. For reference, the three lowest adiabatic PESs are shown in light colors (with a color code similar to the one of Fig. 1).

the region where the nuclear density is considerably different from zero, between $R = -4$ bohr and $R = -1$ bohr, explaining the similarity between $|\Psi(r,R,t)|$ and $|\Psi_{\rm TDSCF}(r,R,t)|$ at this time. At a later time t_2, while $\langle \hat{V} \rangle_\Phi$ is very similar, in shape, to what it was at t_1, the TDPES presents at the same time (*i*) abrupt changes of character, switching from one adiabatic PES to another, and (*ii*) a shape that is very different from its TDSCF counterpart. It is this strong R-dependence of the TDPES that allows for the buildup of a bimodal distribution in the nuclear density (compare with Fig. 1), and, more importantly, that allows for the proper change in the electronic character of the full molecular wavefunction. It is now clear, from the comparison of Figs. 1 and 3 (right panels), that the portion of the wavefunction localized between $R = 4$ bohr and $R = 8$ bohr is associated with the electronic state S_0, as the shape of the TDPES in this region perfectly follows $\epsilon_{BO}^{(S_0)}(R)$, whereas the portion between $R = 1$ bohr and $R = 4$ bohr corresponds to S_1. For smaller values of R a similar analysis is not possible because the nuclear density is too small (see Fig. 1), but the change of electronic character could easily be deduced based on the shape

of the TDPES.

In summary, the comparison between the two product-form expressions of the molecular wavefunction has permitted to shed new lights on the importance of the parametric dependence in the electronic wavefunction. A mean-field expression of the molecular wavefunction, by definition, cannot capture abrupt changes of character on either component of the product. This feature, however, can be reproduced if a parametric dependence of the electronic wavefunction on $\mathbf{R}$ is introduced, that is, if entanglement is correctly accounted for. Note that, in a totally equivalent way, electron-nuclear entanglement can also be expressed via the parametric dependence on $\mathbf{r}$ of the nuclear wavefunction, i.e., $\Psi(\mathbf{r}, \mathbf{R}, t) = \chi_{\mathbf{r}}(\mathbf{R}, t)\Phi(\mathbf{r}, t)$ (this possibility was investigated in Refs. [44, 45, 46]). We also highlight that an analysis of the importance of the parametric nuclear dependence in the context of the (time-independent) BO wavefunction was discussed in Ref. [47].

3. Different flavors of electron-nuclear entanglement

In Section 2 we have analyzed the concept of electron-nuclear entanglement from a quantum-mechanical perspective, by comparing the exact molecular wavefunction to its TDSCF approximation. In this section, we report a similar comparison based on the quantum-classical treatment of the coupled electronic and nuclear dynamics. The motivation for this analysis is the following. The quantum-classical limit of the TDSCF equations yields the well-known Ehrenfest algorithm (see Ref. [13, 15] for derivations). Deriving the equations of motion for Ehrenfest dynamics implies taking the classical limit of the nuclear wavefunction in TDSCF, which has the effect of introducing (what is often noted as) a parametric dependence in the electronic wavefunction. Therefore, we address in this section the question: *Has the classical limit of the nuclear wavefunction the effect of inducing a local entanglement in the electronic wavefunction?* If yes, we would expect better agreement of Ehrenfest results with exact calculations.

To analyze the effect of the classical limit on the nuclear degrees of freedom, we first start by employing the nuclear potential $\langle\hat{V}\rangle_{\tilde{\Phi}} = \langle\hat{V}\rangle_{\tilde{\Phi}}(R, t)$ to propagate classical trajectories, and we compare the resulting distribution of trajectories thus obtained with the distribution of trajectories propagated with the TDPES $\epsilon(R, t)$. Fig. 4 shows the histograms constructed from the classical-trajectory distribution at times t_1 (left panel)

and t_2 (right panel). As a benchmark, we also present the quantum mechanical, TDSCF and exact, nuclear densities. As expected from previous work [36, 48, 38, 49, 39, 50], classical trajectories evolved according to a force that is derived from the exact TDPES perfectly reproduce the quantum mechanical distribution. Analogously, classical trajectories generated *via* the TDSCF nuclear potential $\langle \hat{V} \rangle_{\tilde{\Phi}}$ follow the quantum-mechanical distribution, even though this is not the correct one. According to these proof-of-concept calculations, no major changes are observed in the numerical results in going from the quantum to the quantum-classical approach.

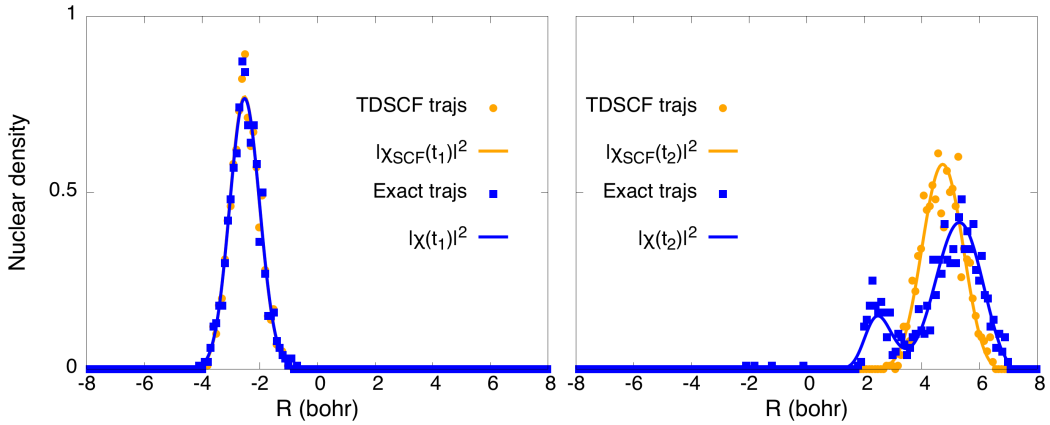

Figure 4: Distribution of classical trajectories evolved according to a force determined from the TDSCF nuclear potential, *i.e.*, $\langle \hat{V} \rangle_{\tilde{\Phi}}(R,t)$ (orange dots), and according to a force determined from $\epsilon(R,t)$ (blue squares), at times $t_1 = 10.8$ fs (left panel) and $t_1 = 31.2$ fs (right panel). For reference, the corresponding quantum probability distributions are shown as continuous lines (orange for TDSCF and blue for the exact one).

Note that the studied test case does not involve phenomena such as multiple passages of the wavepacket through the avoided crossing, which would cause interferences or revival of coherence. However, we have studied in a previous work [39] a case of nonadiabatic quantum interferences, where we also have propagated purely classical trajectories on the exact TDPES. We have concluded that, despite the complex quantum effects taking place during the nonadiabatic interference process, the classical distribution mimics well (at least for short times) the nuclear quantum distribution. This analysis confirmed that the TDPES encodes critical information about the coupled electron-nuclear dynamics, such that classical trajectories propagated on the support of the TDPES capture more

accurately the quantum behavior of nuclei in the presence of nonadiabatic effects than they would do on the support of (time-independent) BO PESs.

Armed with this knowledge, we move towards our final test on Ehrenfest dynamics. Following a standard procedure for the derivation of Ehrenfest equations starting from TDSCF, we replace the nuclear density $|\chi(R,t)|^2$ with a δ-function centered at all times at the position of the classical trajectory $R_{cl}(t)$, *i.e.*, $\delta(R - R_{cl}(t))$. As a result,

$$\langle \hat{V} \rangle_\chi \to \int dR\, V(r,R)\, \delta(R - R_{cl}(t)) = V(r, R_{cl}(t)) \tag{11}$$

and the electronic evolution equation (4) becomes

$$i\hbar\partial_t \tilde{\Phi}_{R_{cl}(t)}(r,t) = \left[\hat{T}_e + V(r, R_{cl}(t))\right] \tilde{\Phi}_{R_{cl}(t)}(r,t). \tag{12}$$

As a consequence of the dependence of the potential on the position of the classical trajectory, $R_{cl}(t)$, triggered by the classical limit performed in Eq. (11), the electronic wavefunction seems to acquire a "point-wise" parametric dependence on the classical position of the nucleus. Such dependence is clearly different from the parametric dependence in $\Phi_R(r,t)$ of Eq. (2), because it introduces only a *local entanglement*, at the position $R_{cl}(t)$, between the electronic and the nuclear wavefunction. Even if a set of trajectories, $R_{cl}^{(I)}(t)$, is considered to mimic the delocalization of the nuclear density, each trajectory I will be locally entangled to the corresponding electronic wavefunction $\Phi_{R_{cl}^{(I)}(t)}(r,t)$. The situation is different if the classical limit is similarly introduced in the electronic equation of motion of the exact factorization (Eq. (7)). A detailed derivation of the quantum-classical equations derived from Eqs. (7) and (8) is beyond the scope of this work, and has been discussed extensively elsewhere [18, 19, 51, 40, 52, 21, 20, 53, 54, 55, 56]. However, it is worth comparing here the effect on Eq. (7) of an operation analogous to what is proposed in Eq. (11). In Eq. (7), the electron-nuclear coupling operator $\hat{U}_{en}[\chi]$ depends explicitly on the nuclear wavefunction $\chi(R,t)$ (and on its gradient), and there is no integral over nuclear coordinates to be performed. Therefore, if a set of trajectories is used to mimic the evolution of the nuclear wavefunction, the electronic equation acquires a dependence on the position of all trajectories. That is, entanglement is *non-local* in the quantum-classical approximation of Eqs. (7) and (8), as is in their exact form.

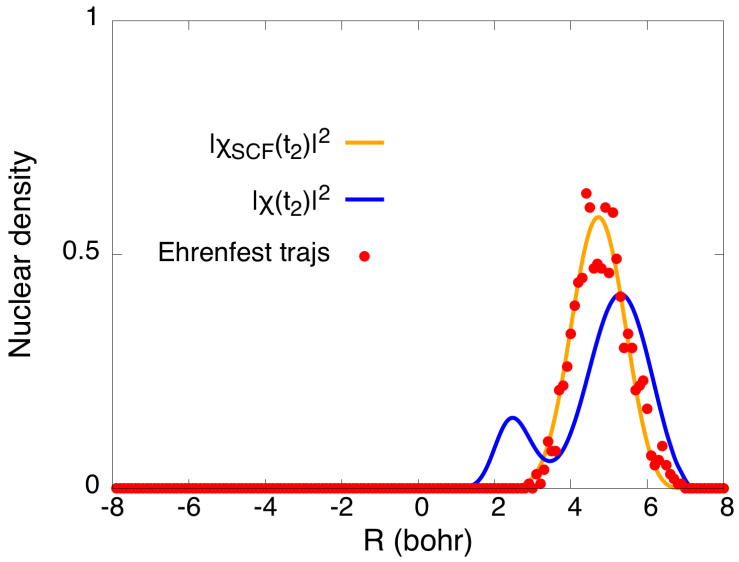

Figure 5: Comparison at time $t_2 = 31.2$ fs of the classical distribution of trajectories propagated according to the Ehrenfest algorithm (red dots), the quantum-mechanical nuclear distribution predicted by TDSCF (orange line), and the exact nuclear distribution (blue line).

To investigate the effect of the local entanglement in Ehrenfest dynamics, we have evolved classical trajectories according to the potential $\langle \hat{V} \rangle_{\tilde{\Phi}_{R_{cl}(t)}}$, where the potential is determined by solving Eq. (12), that is, according to the Ehrenfest algorithm. Fig. 5 shows at time t_2 the distribution of classical trajectories, in comparison to the TDSCF nuclear density and the exact nuclear density. As before, local entanglement does not appear to have a major effect on the nuclear probability distribution. The major issue of this distribution, *i.e.*, the unimodal character, is not cured by the inclusion of entanglement in its local form.

4. Conclusions

We have analyzed the concept of electron-nuclear entanglement in a nonadiabatic process of proton-coupled electron transfer. To this end, we have employed the TDSCF approach, which uses an uncorrelated product Ansatz for the molecular wavefunction composed of an electronic and a nuclear wavefunction, both time-dependent. By construction, TDSCF lacks entanglement between electronic and nuclear variables. This form of

the molecular wavefunction is extremely similar to the exact-factorization expression. However, in the exact factorization the product is not uncorrelated, as the electronic wavefunction depends parametrically on nuclear coordinates. Such dependence is sufficient to restore entanglement in the product form of the molecular wavefunction.

In the present work, we have studied the effect of this parametric dependence on nuclear dynamics, as it can be related to the shape of the potential that drives nuclear evolution. The analysis is presented both at the quantum-mechanical level and within the quantum-classical approximation (when nuclear dynamics is mimicked employing classical trajectories).

In the derivation of the quantum-classical Ehrenfest approach (from TDSCF), we have pointed out what appears as a local parametric dependence of the electronic wavefunction on the position of the classical trajectory. However, such dependence is not enough to restore, not even partially, the entanglement lost in the initial TDSCF Ansatz and fully accounted for in the exact factorization formalism.

Appendix A. Computational details

The model system [41] used for the analysis presented in the main text consists of three ions, two of which are fixed at a distance $L = 20.0$ bohr, and one electron. The mass of the moving ion is $M = 1836$, the proton mass in atomic units; it interacts with the fixed ions via a Coulomb potential and with the electron via a soft-Coulomb potential. The electron interacts with all ions via a soft-Coulomb potential. The potential energy $\hat{V}(r, R)$ in the Hamiltonian describing the system is thus

$$\hat{V} = -\frac{\mathrm{erf}\left(\frac{|R-r|}{R_c}\right)}{|R-r|} - \frac{\mathrm{erf}\left(\frac{\left|r-\frac{L}{2}\right|}{R_r}\right)}{\left|r-\frac{L}{2}\right|} - \frac{\mathrm{erf}\left(\frac{\left|r+\frac{L}{2}\right|}{R_l}\right)}{\left|r+\frac{L}{2}\right|} + \frac{1}{\left|\frac{L}{2}-R\right|} + \frac{1}{\left|\frac{L}{2}+R\right|}. \quad \text{(A.1)}$$

The parameters of the potential have been chosen as $R_c = 4.5$ bohr, $R_l = 4.0$ bohr, and $R_r = 3.0$ bohr.

Quantum-mechanical equations are integrated using the split-operator technique [57] with a time-step of $dt = 0.024$ fs (0.1 au). The initial condition for TDSCF and the exact propagation is $\Psi(r, R, t = 0) = \varphi^{(S_1)}_{R_0}(r) G_\sigma(R - R_0)$ with $\varphi^{(S_1)}_{R_0}(r)$ the S_1 eigenstate of the Hamiltonian $\hat{H}_{BO}$ evaluated at

the nuclear position $R_0 = -4$ bohr, and $G_\sigma(R - R_0) = (\pi\sigma^2)^{-1/4} \exp[-(R - R_0)^2/(2\sigma^2)]$ with $\sigma = 0.3$ bohr. Classical trajectories are also propagated with a time-step of $dt = 0.024$ fs (0.1 au) in all cases, namely when the trajectories are evolved on $\langle \hat{V} \rangle_{\tilde{\Phi}}(R, t)$ or on the TDPES, and within the Ehrenfest propagation. For all quantum-classical simulations, 200 trajectories have been employed, sampled from the Wigner distribution corresponding to the quantum-mechanical nuclear probability density.

In order to determine the TDPES of Eqs. (7) and (8), the time-dependent Schrödinger equation for $\Psi(r, R, t)$ has been solved. Having access to the full wavefunction, the nuclear density is easily derived from the integral over the electronic variable of $|\Psi(r, R, t)|^2$. The phase $S(R, t)$ of the nuclear wavefunction, from the expression $\chi = |\chi| \exp[(i/\hbar)S]$, is determined [38] according to

$$S(R, t) = \int^R dR' \frac{\mathrm{Im}\langle \Psi(R', t) | \partial_{R'} | \Psi(R', t) \rangle_r}{|\chi(R', t)|^2}, \tag{A.2}$$

which guarantees that the time-dependent vector potential of the theory is identically zero at all times. The electronic wavefunction to be used in Eq. (9) is determined as $\Phi_R(r, t) = \Psi(r, R, t)/\chi(R, t)$. Note that there might be regions where the nuclear density is very small or zero. To circumvent this numerical issue, we compute R-dependent quantities only in the regions where $|\chi(R, t)| > 10^{-8}$. We dot not expect that this operation strongly affects the overall behavior of the ensemble of trajectories, since classical trajectories are to be found in regions of large probability. Furthermore, diverging trajectories can be neglected in the calculations of average quantities, as the trajectories are propagated independently.

It is worth mentioning here that a quantum-classical algorithm has been derived based on the exact-factorization equations and allows for the on-the-fly calculations of the TDPES without the need to solve the full time-dependent Schrödinger equation. It has been applied to the study of model systems [52, 21, 55, 19, 18] and of the photoactivated dynamics in isolated molecules [51, 56, 40, 20]. The algorithm, dubbed coupled-trajectory mixed quantum-classical (CT-MQC), is designed to solve the electronic equation of the exact factorization to determine the TDPES, which in turn is used to propagate classical trajectories. The electronic evolution operator depends explicitly on the nuclear wavefunction. Therefore, at each step of dynamics, the distribution of classical trajectories

is employed to construct an approximate form of the nuclear wavefunction. This operation requires that the trajectories are propagated simultaneously. We expect that at short times the classical distribution remains close to what would be the quantum nuclear distribution, but this cannot guaranteed at longer times.

Appendix B. Derivation of the TDSCF equations

In order to derive expressions (4) and (5) starting from the TDSCF Ansatz for the molecular wavefunction, we have used the following form:

$$\Psi_{\rm TDSCF}(r,R,t) = \chi(R,t)\Phi(r,t)e^{\frac{i}{\hbar}\int_0^t dt'\, E_{BO}(t')} = \chi(R,t)\tilde{\Phi}(r,t), \qquad \text{(B.1)}$$

with

$$E_{BO}(t) = \int dr\, \Phi^*(r,t) i\hbar\partial_t \Phi(r,t). \qquad \text{(B.2)}$$

Clearly, multiplying the full wavefunction of Eq. (1) by a purely time-dependent phase factor does not affect observable properties, but it allows to derive a symmetric form of the evolution equations for $\chi(R,t)$ and $\tilde{\Phi}(r,t)$.

We insert Eq. (B.1) into the time-dependent Schrödinger equation (3). We then project onto $\Phi^*(r,t)$,

$$\begin{aligned} i\hbar\partial_t\chi(R,t) &= \left[\hat{T}_n + \langle\hat{V}\rangle_\Phi\right]\chi(R,t) + \langle\hat{T}_e\rangle_\Phi\chi(R,t) \\ &\quad + \left[E_{BO}(t) - \int dr\, \Phi^*(r,t) i\hbar\partial_t\Phi(r,t)\right]\chi(R,t), \end{aligned} \qquad \text{(B.3)}$$

and onto $\chi^*(R,t)$

$$\begin{aligned} i\hbar\partial_t\Phi(r,t) &= \left[\hat{T}_e + \langle\hat{V}\rangle_\chi\right]\Phi(r,t) + \langle\hat{T}_n\rangle_\chi\Phi(r,t) \\ &\quad + \left[E_{BO}(t) - \int dR\, \chi^*(R,t) i\hbar\partial_t\chi(R,t)\right]\Phi(r,t), \end{aligned} \qquad \text{(B.4)}$$

where we have imposed the normalization of the two wavefunctions. In order to simplify the equations just derived, we note that the total energy of the electron-nuclear system, E, is

$$E = \int dr \int dR\, \chi^*(R,t)\tilde{\Phi}^*(r,t) i\hbar\partial_t\, \chi(R,t)\tilde{\Phi}(r,t), \qquad \text{(B.5)}$$

which follows from the Schrödinger equation. Thus

$$E = \int dR\, \chi^*(R,t) i\hbar\partial_t\, \chi(R,t) + \int dr\, \Phi^*(r,t) i\hbar\partial_t\, \Phi(r,t) - E_{BO}(t). \quad \text{(B.6)}$$

It follows from our choice of $E_{BO}(t)$ that the first term in Eq. (B.6) equals the total energy of the system E.

The nuclear evolution equation (B.3) reduces to Eq. (5) once the constant (as a function of R) term $\langle \hat{T}_e \rangle_\Phi$ is neglected, having no effect on the dynamics. Similarly, thanks to the relation

$$\Big[i\hbar\partial_t\, \Phi(r,t) - E_{BO}(t)\Phi(r,t) \Big] e^{\frac{i}{\hbar}\int_0^t dt'\, E_{BO}(t')} = i\hbar\partial_t\, \tilde{\Phi}(r,t), \quad \text{(B.7)}$$

the electronic evolution equation (B.4) reduces to Eq. (4), if we neglect the constant (as function of r) term $\langle \hat{T}_n \rangle_\chi - E$.

References

[1] A. D. McLachlan, M. A. Ball, Time-dependent Hartree-Fock theory of molecules, Rev. Mod. Phys. 36 (1964) 844.

[2] J. W. Negele, The mean-field theory of nuclear structure and dynamics, Rev. Mod. Phys. 54 (1982) 913.

[3] R. A. Harris, On a time dependent Hartree theory of anharmonically coupled oscillators, J. Chem. Phys. 72 (1980) 1776.

[4] M. Messina, R. D. Coalson, Timedependent Hartree wave packet dynamical techniques for computation of electronically excited state optical spectra of manybody quantum systems, J. Chem. Phys. 90 (1989) 4015.

[5] P. Jungwirth, R. B. Gerber, Quantum molecular dynamics of ultrafast processes in large polyatomic systems, Chem. Rev. 99 (1999) 1583.

[6] R. B. Gerber, V. Buch, M. A. Ratner, Timedependent selfconsistent field approximation for intramolecular energy transfer. I. Formulation and application to dissociation of van der Waals molecules, J. Chem. Phys. 77 (1982) 3022.

[7] N. Makri, W. H. Miller, Timedependent selfconsistent field (TD-SCF) approximation for a reaction coordinate coupled to a harmonic bath: Single and multiple configuration treatments, J. Chem. Phys. 87 (1987) 5781.

[8] R. Schinke, Photodissociation dynamics: spectroscopy and fragmentation of small polyatomic molecules, no. 1, Cambridge University Press, 1995.

[9] L. Zhang, S.-Y. Lee, D. H. Zhang, A test of the Continuous Configuration Time-Dependent Self-Consistent Field (CC-TDSCF) method on the H+CH_4 reaction, J. Phys. Chem. A 110 (2006) 5513.

[10] H. D. Meyer, U. Manthe, L. S. Cederbaum, The multi-configurational time-dependent Hartree approach, Chem. Phys. Lett. 165 (1990) 73–78.

[11] G. A. Worth, H.-D. Meyer, H. Köppel, L. S. Cederbaum, I. Burghardt, Using the MCTDH wavepacket propagation method to describe multimode non-adiabatic dynamics, Int. Rev. Phys. Chem. 27 (3) (2008) 569–606.

[12] G. A. Worth, H. D. Meyer, L. S. Cederbaum, Multidimensional dynamics involving a conical intersection: Wavepacket calculations using the MCTDH method, in: W. Domcke, D. R. Yarkony, H. Köppel (Eds.), Conical Intersections: Electronic Structure, Dynamics & Spectroscopy, Vol. 15 of Advanced Series in Physical Chemistry, 2004, Ch. 14, pp. 583–617.

[13] J. C. Tully, Mixed quantum-classical dynamics: mean-field and surface-hopping, in: B. J. Berne, G. Ciccotti, D. F. Coker (Eds.), Classical and Quantum Dynamics in Condensed Phase Simulations, Singapore, World Scientific, 1998.

[14] G. S. Whittier, J. C. Light, Quantum/classical time-dependent self-consistent field treatment of Ar+HCO inelastic and dissociative scattering, J. Chem. Phys. 110 (1999) 4280.

[15] D. Marx, J. Hutter, Ab Initio Molecular Dynamics: Basic Theory and Advanced Methods, Cambridge University Press, 2009.

[16] M. Vacher, M. J. Bearpark, M. A. Robb, Direct methods for non-adiabatic dynamics: connecting the single-set variational multi-configuration Gaussian (vMCG) and Ehrenfest perspectives, Theor. Chem. Acc. 135 (2016) 187.

[17] P. Lopez-Tarifa, M.-A. Herve du Penhoat, R. Vuilleumier, M.-P. Gaigeot, I. Tavernelli, A. Le Padellec, J.-P. Champeaux, M. Alcami, P. Moretto-Capelle, F. Martin, M.-F. Politis, Ultrafast nonadiabatic fragmentation dynamics of doubly charged uracil in a gas phase, Phys. Rev. Lett. 107 (2011) 023202.

[18] S. K. Min, F. Agostini, E. K. U. Gross, Coupled-trajectory quantum-classical approach to electronic decoherence in nonadiabatic processes, Phys. Rev. Lett. 115 (7) (2015) 073001.

[19] F. Agostini, S. K. Min, A. Abedi, E. K. U. Gross, Quantum-classical non-adiabatic dynamics: Coupled- vs. independent-trajectory methods, J. Chem. Theory Comput. 12 (5) (2016) 2127–2143.

[20] B. F. E. Curchod, F. Agostini, I. Tavernelli, CT-MQC – A coupled-trajectory mixed quantum/classical method including nonadiabatic quantum coherence effects, Euro. Phys. J. B 91 (2018) 168.

[21] F. Agostini, An exact-factorization perspective on quantum-classical approaches to excited-state dynamics, Euro. Phys. J. B 91 (2018) 143.

[22] J. L. Alonso, P. Bruscolini, A. Castro, J. Clemente-Gallardo, J. C. Cuchí, J. A. Jover-Galtier, Ehrenfest statistical dynamics in chemistry: Study of decoherence effects, J. Chem. Theory Comput. 14 (2018) 3975.

[23] A. P. Horsfield, D. R. Bowler, A. J. Fisher, T. N. Todorov, M. J. Montgomery, Power dissipation in nanoscale conductors: classical, semi-classical and quantum dynamcis, J. Phys.: Condens. Matter 16 (2004) 3609.

[24] P. V. Parandekar, J. C. Tully, Mixed quantum-classical equilibrium, J. Chem. Phys. 122 (2005) 094102.

[25] P. V. Parandekar, J. C. Tully, Detailed balance in ehrenfest quantum-classical dynamics, J. Chem. Theory Comput. 2 (2006) 229.

[26] J. L. Alonso, A. Castro, J. Clemente-Gallardo, J. C. Cuchí, P. Echenique, F. Falceto, Statistics and nosé formalism for Ehrenfest dynamics, Journal of Physics A: Mathematical and Theoretical 44 (2011) 395004.

[27] A. Jain, J. E. Subotnik, Vibrational energy relaxation: A benchmark for mixed quantum-classical methods, J. Phys. Chem. A 122 (2018) 16.

[28] T. Yonehara, K. Hanasaki, K. Takatsuka, Fundamental approaches to nonadiabaticity: Toward a chemical theory beyond the Born-Oppenheimer paradigm, Chem. Rev. 112 (1) (2012) 499–542.

[29] D. Shalashilin, Quantum mechanics with the basis set guided by ehrenfest trajectories: Theory and application to spin-boson model, J. Chem. Phys. 130 (2009) 244101.

[30] A. J. Jenkins, K. E. Spinlove, M. Vacher, G. A. Worth, M. A. Robb, The Ehrenfest method with fully quantum nuclear motion (Qu-Eh): Application to charge migration in radical cations, J. Chem. Phys. 149 (2018) 094108.

[31] A. Abedi, N. T. Maitra, E. K. U. Gross, Exact factorization of the time-dependent electron-nuclear wave function, Phys. Rev. Lett. 105 (12) (2010) 123002.

[32] A. Abedi, N. T. Maitra, E. K. U. Gross, Correlated electron-nuclear dynamics: Exact factorization of the molecular wave-function, J. Chem. Phys. 137 (22) (2012) 22A530.

[33] F. G. Eich, F. Agostini, The adiabatic limit of the exact factorization of the electron-nuclear wave function, J. Chem. Phys. 145 (2016) 054110.

[34] A. Scherrer, F. Agostini, D. Sebastiani, E. K. U. Gross, R. Vuilleumier, Nuclear velocity perturbation theory for vibrational circular dichroism: An approach based on the exact factorization of the electron-nuclear wave function, J. Chem. Phys. 143 (7) (2015) 074106.

[35] A. Scherrer, F. Agostini, D. Sebastiani, E. K. U. Gross, R. Vuilleumier, On the mass of atoms in molecules: Beyond the born-oppenheimer approximation, Phys. Rev. X 7 (2017) 031035.

[36] F. Agostini, A. Abedi, Y. Suzuki, E. K. U. Gross, Mixed quantum-classical dynamics on the exact time-dependent potential energy surfaces: A novel perspective on non-adiabatic processes, Mol. Phys. 111 (22-23) (2013) 3625.

[37] A. Abedi, F. Agostini, Y. Suzuki, E. K. U. Gross, Dynamical steps that bridge piecewise adiabatic shapes in the exact time-dependent potential energy surface, Phys. Rev. Lett 110 (26) (2013) 263001.

[38] F. Agostini, A. Abedi, Y. Suzuki, S. K. Min, N. T. Maitra, E. K. U. Gross, The exact forces on classical nuclei in non-adiabatic charge transfer, J. Chem. Phys. 142 (8) (2015) 084303.

[39] B. F. E. Curchod, F. Agostini, E. K. U. Gross, An exact factorization perspective on quantum interferences in nonadiabatic dynamics, J. Chem. Phys. 145 (2016) 034103.

[40] F. Agostini, B. F. E. Curchod, R. Vuilleumier, I. Tavernelli, E. K. U. Gross, Tddft and quantum-classical dynamics: A universal tool describing the dynamics of matter, in: W. Andreoni, S. Yip (Eds.), Handbook of Materials Modeling, Springer Netherlands, 2018, pp. 1–47.

[41] S. Shin, H. Metiu, Nonadiabatic effects on the charge transfer rate constant: A numerical study of a simple model system, J. Chem. Phys. 102 (23) (1995) 9285–9295.

[42] B. F. E. Curchod, F. Agostini, On the dynamics through a conical intersection, J. Phys. Chem. Lett. 8 (2017) 831.

[43] F. Agostini, B. F. E. Curchod, When the exact factorization meets conical intersections..., Euro. Phys. J. B 91 (2018) 141.

[44] Y. Suzuki, A. Abedi, N. T. Maitra, K. Yamashita, E. K. U. Gross, Electronic Schrödinger equation with nonclassical nuclei, Phys. Rev. A 89 (4) (2014) 040501(R).

[45] E. Khosravi, A. Abedi, N. T. Maitra, Exact potential driving the electron dynamics in enhanced ionization of H_2^+, Phys. Rev. Lett. 115 (2015) 263002.

[46] E. Khosravi, A. Abedi, A. Rubio, N. T. Maitra, Electronic non-adiabatic dynamics in enhanced ionization of isotopologues of hydrogen molecular ions from the exact factorization perspective, Phys. Chem. Chem. Phys. 19 (2017) 8269.

[47] A. F. Izmaylov, I. Franco, Entanglement in the born-oppenheimer approximation, J. Chem. Theory Comput. 13 (2017) 20.

[48] Y. Suzuki, A. Abedi, N. T. Maitra, E. K. U. Gross, Laser-induced electron localization in H_2^+: Mixed quantum-classical dynamics based on the exact time-dependent potential energy surface, Phys. Chem. Chem. Phys. 17 (2015) 29271–29280.

[49] F. Agostini, S. K. Min, E. K. U. Gross, Semiclassical analysis of the electron-nuclear coupling in electronic non-adiabatic processes, Ann. Phys. 527 (9-10) (2015) 546–555.

[50] Y. Suzuki, K. Watanabe, Bohmian mechanics in the exact factorization of electron-nuclear wave functions, Phys. Rev. A 94 (2016) 032517.

[51] S. K. Min, F. Agostini, I. Tavernelli, E. K. U. Gross, Ab initio nonadiabatic dynamics with coupled trajectories: A rigorous approach to quantum (de)coherence, J. Phys. Chem. Lett. 8 (2017) 3048.

[52] G. Gossel, F. Agostini, N. T. Maitra, Coupled-trajectory mixed quantum-classical algorithm: A deconstruction, J. Chem. Theory Comput. 14 (2018) 4513.

[53] F. Agostini, A. Abedi, E. K. U. Gross, Classical nuclear motion coupled to electronic non-adiabatic transitions, J. Chem. Phys. 141 (21) (2014) 214101.

[54] A. Abedi, F. Agostini, E. K. U. Gross, Mixed quantum-classical dynamics from the exact decomposition of electron-nuclear motion, Europhys. Lett. 106 (3) (2014) 33001.

[55] F. Agostini, I. Tavernelli, G. Ciccotti, Nuclear quantum effects in electronic (non)adiabatic dynamics, Euro. Phys. J. B 91 (2018) 139.

[56] J.-K. Ha, I. S. Lee, S. K. Min, Surface hopping dynamics beyond nonadiabatic couplings for quantum coherence, J. Phys. Chem. Lett. 9 (2018) 1097.

[57] M. D. Feit, F. A. Fleck Jr., A. Steiger, Solution of the Schrödinger equation by a spectral method, J. Comput. Phys. 47 (1982) 412.